Indian Journal of Chemistry
Vol. 56A, January 2017, pp. 50-56

Notes

Synthesis and characterization of gadolinium tungstate doped zinc oxide photocatalyst

Kuppulingam Thirumalai[a], Manohar Shanthi[a] & Meenakshisundaram Swaminathan*[, a, b]

[a]Photocatalysis Laboratory, Department of Chemistry, Annamalai University, Annamalai Nagar 608 002, Tamil Nadu, India

[b]Department of Chemistry, International Research Centre, Kalasalingam University, Krishnan Kovil 626 126, India

Email: chemres50@gmail.com; m.swaminathan@klu.ac.in

Received 19 December 2016; accepted 30 December 2016

Fabrication of 5 wt% Gd_2WO_6 doped ZnO via template-free hydrothermal process and its photocatalytic activity against azo dyes, rhodamine-B (Rh–B) and trypan blue (TB) in UV-A light irradiation are reported. The as-prepared Gd_2WO_6 doped ZnO has been characterised by X-ray diffraction, field emission scanning electron microscopy, X-ray photoelectron spectroscopy, and, diffused reflectance and photoluminescence spectroscopy. The XRD pattern indicates the distinct diffraction peaks for wurtzite ZnO and body-centered monoclinic structure of Gd_2WO_6 with good crystallinity. EDS analysis reveals the homogeneous distribution of Gd, Zn, W and O in the prepared catalyst. The results suggests that rare earth tungstate, Gd_2WO_6 doping on ZnO has great influence on the photocatalytic activity under UV-A light. Gd_2WO_6-ZnO possesses high reusability without appreciable loss of catalytic activity up to four runs.

Keywords: Photocatalysis, Zinc oxide, Wurtzite structure, Semiconductor oxides, Gadolinium tungstate, Degradation, Dye degradation, Rhodamine B

The removal of organic pollutants is of particular importance due to their harmful effect on the environment. Though various physical, chemical and biological techniques are widely used in removal of organic pollutants, advanced oxidation processes (AOPs) have gained attention as an alternative to traditional treatment processes for organic pollutant removal.[1-3] In AOP processes, semiconductor-mediated heterogeneous photocatalysis is a promising, valuable technique for environmental and energy applications.[4,5] ZnO is a II-VI semiconductor oxide and has a wurtzite structure with a direct wide band gap of 3.37 eV and a large exciton binding energy of 60 meV at room temperature. Doping of metal oxide to the ZnO matrix may introduce the shallow or deep-level states with slight changes in the band gap, and increase the photocatalytic activity in visible-light region.[6-10]

Compounds of the rare earth tungstate and molybdate families have a long history of practical applications due to their unique luminescence properties, resulting from the orbital hybridization of $4f$ electrons.[11,12] Some of the reports are available for Gd doped ZnO for light-emitting displays, catalysis, drug delivery, ethanol sensing, and optical storage devices due to their temperature independent luminescence in ultraviolet (UV) and visible light.[13,14] Gd doped ZnO has been found to be controlled by external magnetic field and temperature. The average magnetic moment per Gd atom is as high as 3278 μB which can be used in the production of ZnO based electronic devices.[15] Gadolinium doped titania showed significantly higher photocatalytic activity than the undoped titania.[16] Gadolinium tungstate (Gd_2WO_6) and molybdate (Gd_2MoO_6) have attracted much interest for their remarkable properties such as ferroelectricity, laser hosts, phosphors and catalysis.[17-19] Here we report the successful synthesis of Gd_2WO_6 doped ZnO for enhanced photocatalysis in azo dye degradation under UV-A light.

Experimental

Zinc nitrate hexahydrate ($Zn(NO_3)_2.6H_2O$, gadolinium nitrate pentahydrate $Gd(NO_3)_3{\cdot}5H_2O$, sodium tungstate dihydrate ($Na_2WO_4.2H_2O$), oxalic acid dihydrate ($C_2H_2O_4.2H_2O$) and methanol (CH_3OH) (HPLC grade) were obtained from Himedia Chemicals. Rhodamine B ($C_{28}H_{31}ClN_2O_3$; mol. wt. 479.01), trypan blue (TB, $C_{34}H_{28}N_6O_{14}S_4$ mol. wt. 872.88) from Colour Chem, Pondicherry and ZnO (surface area 5 m^2/g; particle size 4.80 μm) from Merck Chemicals were used as received. Deionized distilled water was employed throughout the experiments.

$Na_2WO_4.2H_2O$ (0.05 *M*, 1.649 g) was dissolved in 100 mL of deionized water. Under vigorous agitation, 0.243 g of $Gd(NO_3)_3.5H_2O$ solution (0.05 *M*) was added into the Na_2WO_4 solution at room temperature. The pH of the solution was adjusted to 10 with NaOH for the complete precipitation of Gd_2WO_6. The Gd_2WO_6 suspension was mixed with 100 mL 0.4 *M* $Zn(NO_3)_2{\cdot}6H_2O$ (11.90 g) solution and stirred for 30 min. Then, 100 mL of oxalic acid in distilled water (0.6 *M*) was added to the above solution drop-wise

and stirred for 4 h to ensure complete precipitation of zinc oxalate. The mixed precipitate of zinc oxalate and Gd_2WO_6 was treated hydrothermally in a Teflon lined stainless steel autoclave at 115 °C for 12 h under a pressure of 18 psi. The hydrothermally treated precipitate was dried in air at 90 °C for 12 h and calcined at 450 °C for 12 h in a muffle furnace to obtain 5 wt% of Gd_2WO_6 in ZnO**.** In the above procedure, appropriate amounts of $Gd(NO_3)_3.5H_2O$ and $Na_2WO_4.2H_2O$ were used to get 3 wt% and 9 wt% of Gd_2WO_6 loaded ZnO.

X-ray diffraction (XRD) patterns were recorded with a Siemens D5005 diffractometer using Cu-Kα (k = 0.151 418 nm) radiation. Maximum peak positions were compared with the standard files to identity the crystalline phase. The surface morphology of the Gd_2WO_6-ZnO was studied by using a field emission scanning electron microscope (FE-SEM) (model Ultra-55). EDS analysis was performed on gold coated samples using a FE-SEM (model ULTRA–55). X-ray photoelectron spectra (XPS) of the catalysts were recorded on an ESCA-3 Mark II spectrometer (VG Scientific Ltd., England) using Al-Kα (1486.6 eV) radiation as the source. The spectra were referenced to the binding energy of C (1*s*) (285 eV). A Perkin Elmer LS 55 fluorescence spectrometer was employed to record the photoluminescence (PL) spectra at room temperature. Diffuse reflectance spectra were recorded with Shimadzu UV-2450. UV absorbance measurements were made using Hitachi-U-2001 spectrometer.

All experiments were carried out under identical conditions using a Heber multilamp photoreactor (model HML-MP 88). The irradiation was carried out using four parallel medium pressure mercury lamps emitting light at 365 nm wavelength. An open borosilicate glass tube of 40 cm height and 20 mm diameter was used as the reaction vessel. The dye solution (50 mL) and Gd_2WO_6-ZnO (150 mg) were taken in the reaction tube and irradiated. Prior to irradiation, the reaction mixture was continuously aerated by a pump to provide oxygen and to attain adsorption-desorption equilibrium between the dye and Gd_2WO_6-ZnO. During the illumination time, no volatility of the solvent was observed. After dark adsorption, the first sample was taken. At specific time intervals, 2 mL of the sample was withdrawn and centrifuged to separate the catalyst. Then, 1 mL of the centrifugate was diluted to 10 mL and its absorbance was measured at 259 and 236 nm for Rh-B and TB dyes respectively. Chemical structures of dyes are given in Fig. S1 (Supplementary data). The absorbencies at 259 and 236 nm represent the aromatic content of Rh-B and TB respectively and their decrease indicate the degradation of dye.

Results and discussion

XRD is an effective non-destructive tool for qualitative and quantitative analysis of the phase structure. Figure 1 shows the XRD patterns of the Gd_2WO_6-ZnO. The diffraction peaks of ZnO at 32.11, 34.47, 36.31, 47.56, 56.73, 62.75, 66.67, 67.98, 69.02, 72.96, and 77.13° correspond to (100), (002), (101), (102), (110), (103), (220), (112), (201), (004) and (202) planes of wurtzite ZnO (Fig. 1a) (JCPDS no. 36–1451). The diffraction peaks at 22.64, 23.96, 27.88 and 30.50 for the planes (211), (130), (321) and (411) in Fig. 1b are due to the body-centered monoclinic structure of Gd_2WO_6 (JCPDS no. 23–1074). The Gd_2WO_6 phase is more stable at ambient temperature in air. The Scherrer formula ($\Phi = K\lambda/\beta\cos\theta$, where Φ is the crystallite size, λ is the wavelength of X-ray, *K* is the shape factor, β is the full line width at the half-maximum height of the peak, and θ is the Bragg angle.) was used for the calculation of the average crystallite size of Gd_2WO_6-ZnO. Particles size was calculated using all the intense peaks. The average crystallite size of Gd_2WO_6-ZnO was found to be 24.2 nm.

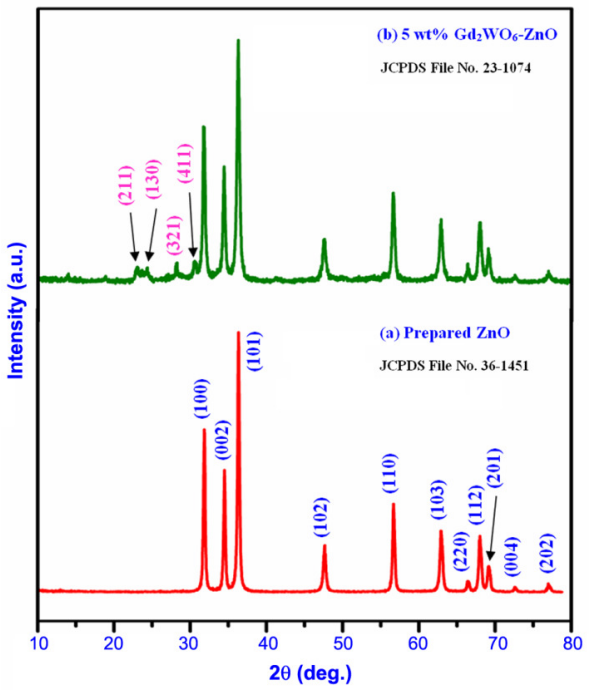

Fig 1–XRD patterns of (a) prepared ZnO and (b) 5 wt% Gd_2WO_6-ZnO.

Electronic microscopy is a technique widely used in structural and chemical characterizations to get information about morphology, grain size, chemical composition and crystallinity of materials. Figure 2 depicts FE-SEM images at different magnifications of Gd_2WO_6-ZnO giving typical information about its morphological features. It reveals that hydrothermal treatment has a significant effect on the morphology of prepared catalyst. Figure 2a clearly shows that Gd_2WO_6-ZnO has the morphology of combined nanorods and microsponge-like structure with a number of cavities. Regularly arranged nanoclusters are clearly seen in Fig. 2b. These morphological features of Gd_2WO_6-ZnO are responsible for the enhanced photocatalytic activity. The presence of elements Gd, Zn, W and O in the catalyst is revealed by EDS recorded from the selected area (Fig. 3). It is seen that the intensity of Zn peak is higher than those of the peaks of the other elements. EDS spectrum further confirms the purity of the prepared catalyst, since there is no peak for any other elements.

XPS is a selective and sensitive surface characterization technique to determine the chemical compositions of materials, and it is also effective in investigating the characteristics (valence) of the constituent atoms (ions) by monitoring their binding energies. The survey spectrum of Gd_2WO_6-ZnO photocatalyst mainly consists of zinc, gadolinium, carbon, oxygen and tungsten species (Fig. 4a). No additional peaks were observed. An XPS spectrum of Zn 2*p* is shown in Fig. 4b; the peaks of Zn $2p_{1/2}$ and Zn $2p_{3/2}$ are located at 1045.7 and 1022.5 eV respectively. From the peak positions we can conclude that Zn is in the state of Zn^{2+}(ref. 20) Figure 4c shows the XPS spectra of gadolinium with valance states of Gd 3*d* wherein the peak positions of Gd $3d_{5/2}$ and Gd$3d_{3/2}$ are placed at binding energies of 1196.8 and 1225.9 eV respectively. This indicates gadolinium ions are present in +3 oxidation state.[21] The W $4f_{5/2}$ and W $4f_{7/2}$ peaks (Fig. 4d) centred at 36.6 and 38.7 eV are assigned to W^{6+} of Gd_2WO_6 which is confirmed by the reported values.[22] Binding energy peak of O1*s* is asymmetric and can be fitted to two symmetrical peaks (locating at 531.4 and 532.8 eV) (Fig. 4e), for two different kinds of O species in the sample. These two peaks should be associated with the lattice oxygen (OL) of Gd_2WO_6-ZnO and chemisorbed oxygen (OH) caused by the surface hydroxyl.

To study the optical characteristics, UV-vis diffuse reflectance and photoluminescence spectra for the ZnO and Gd_2WO_6–ZnO catalysts were recorded. Gd_2WO_6-ZnO shows an increased absorption over the undoped ZnO material both in the visible and the ultraviolet regions (Fig. 5). UV-vis spectra in the diffuse reflectance mode (R) were transformed to the

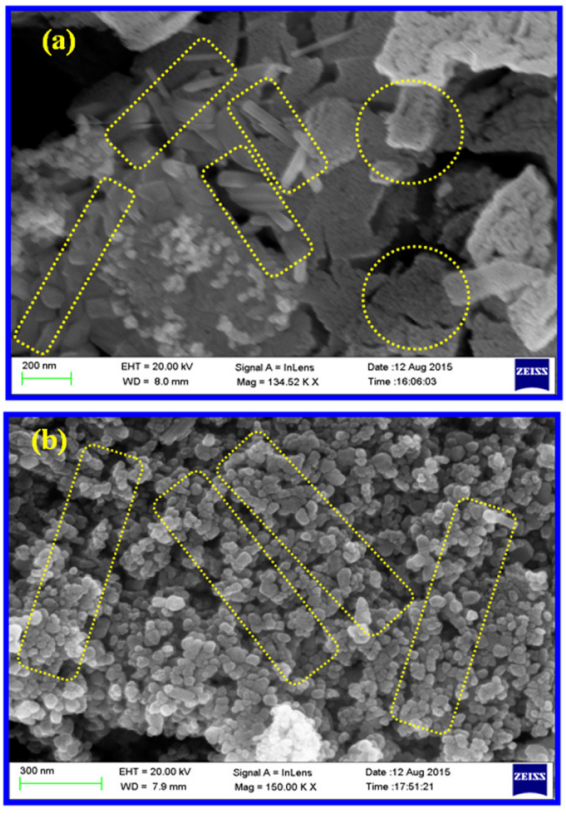

Fig 2–FE-SEM of Gd_2WO_6-ZnO at different magnification. [(a) 200 nm and (b) 300 nm].

No	Element	Series	unn. C (wt.%)	norm. C (wt.%)	Atom. C (wt.%)	Error (3 σ)
1	Zn	K	45.89	38.46	8.90	4.03
2	O	K	35.94	30.12	19.59	3.13
3	W	L	31.48	26.39	70.15	12.59
4	Gd	L	6.00	5.03	1.36	0.64
		Total	119.30	100.00	100.00	

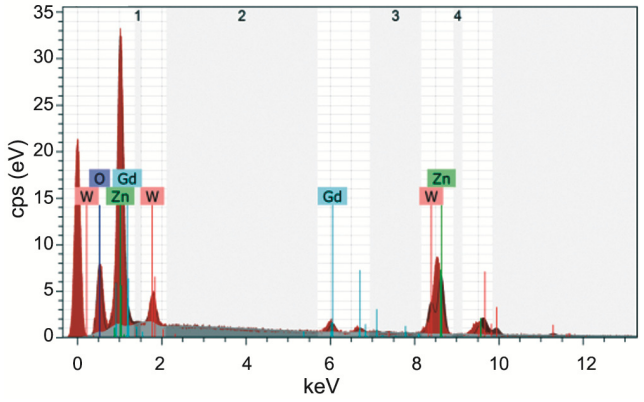

Fig 3–EDS spectrum of Gd_2WO_6-ZnO.

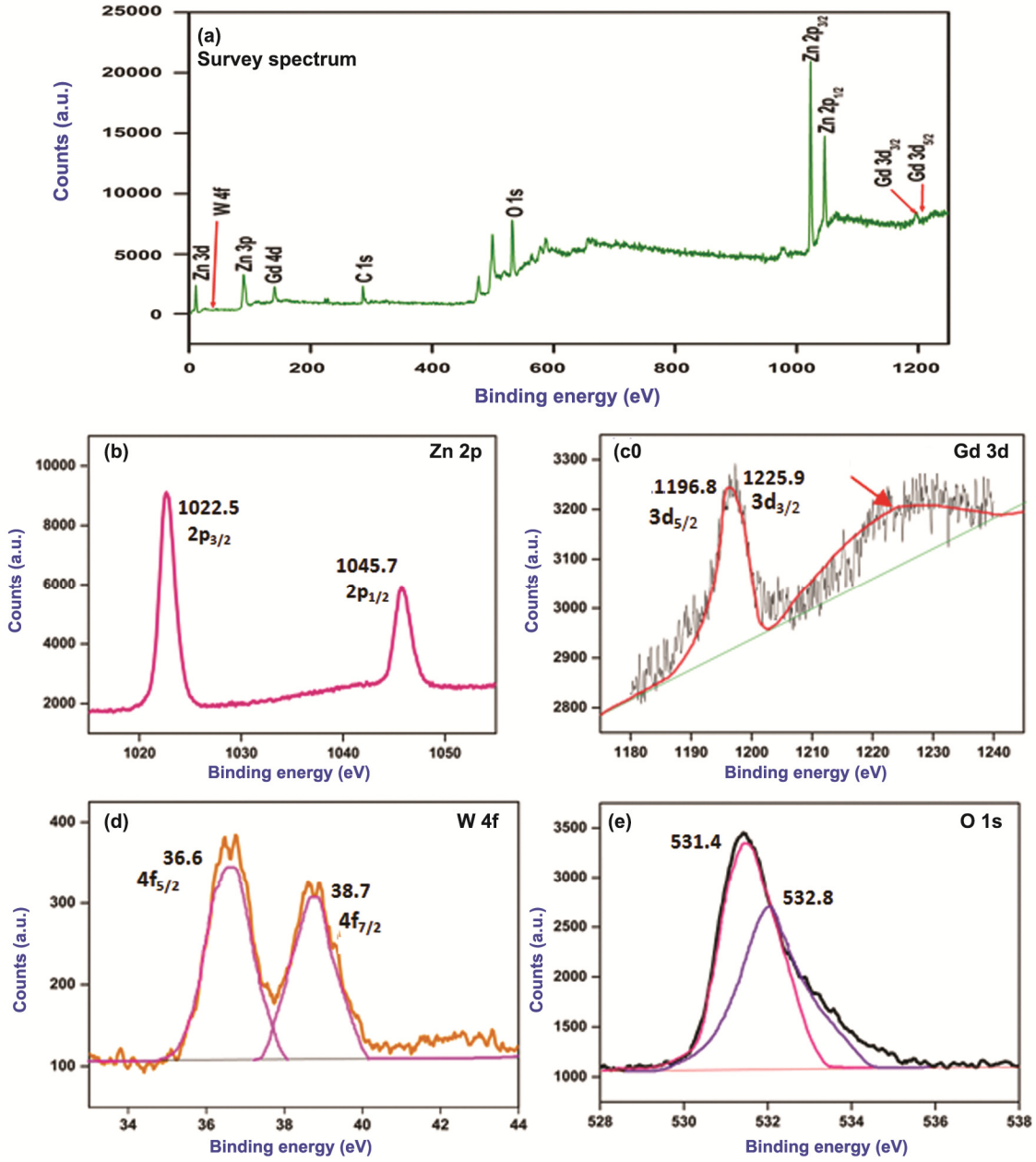

Fig 4–XPS analysis of Gd_2WO_6-ZnO. [(a) Survey spectrum, (b) Zn 2*p*, (c) Gd 3*d*, (d) W 4*f* and (e) O 1*s*.

Kubelka-Munk function F(R) to separate the extent of light absorption from scattering. The band gap energy was obtained from the plot of the modified Kubelka-Munk function $(F(R)E)^{1/2}$ versus the energy of the absorbed light E ($(F(R)E)^{1/2} = [((1–R)^2/2R)\times h\upsilon]$.

Band gap energies for the prepared ZnO and Gd_2WO_6-ZnO are 3.15 and 2.93 eV respectively (Supplementary data, Figs S2(a, b)). Any impurity in the semiconductor oxide can form intermittent band energy levels and this leads to the decrease of bandgap energy, which increases the visible absorption. Reduction of bandgap energy by the addition of Gd^{3+} has been reported earlier.[23]

The photoluminescence spectra has been utilised for studying the separation of the photogenerated electron-hole pair. The fluorescence emission is mostly from the recombination of the photogenerated electron-hole pairs, which is related to photocatalytic activity. Figure 6 presents the photoluminescence spectra of the prepared ZnO and Gd_2WO_6-ZnO. The

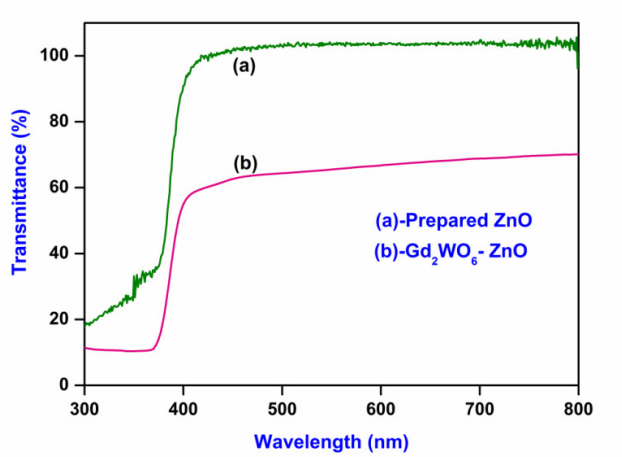

Fig 5–Diffused reflectance spectrum of prepared ZnO (curve a) and Gd_2WO_6 doped ZnO (curve b).

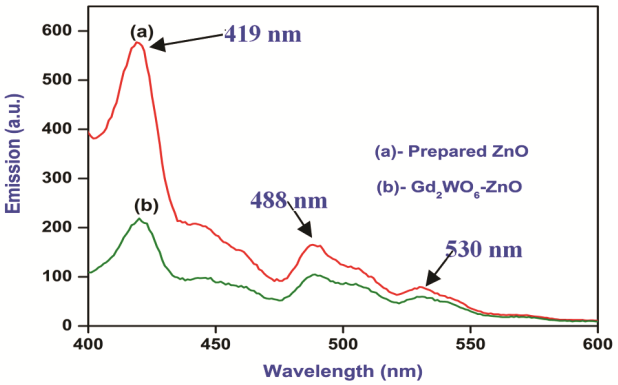

Fig 6–Photoluminescence spectrum of prepared ZnO (curve a) and Gd_2WO_6 doped ZnO (curve b).

excitation wavelength is 370 nm and emission was observed at 419, 488 and 530 nm. They can be ascribed to $^7F_0$–$^5D_3$, $^7F_0$–$^5D_2$ and $^7F_0$–$^5D_1$.[24] It can be seen that the peak positions are similar for ZnO and Gd_2WO_6-ZnO, while PL intensities are different. The PL of prepared ZnO at 419 nm is due to electron-hole recombination and its intensity is higher than Gd_2WO_6-ZnO. The decreased emission intensity in Gd_2WO_6-ZnO implies that the recombination of charge carriers is suppressed by Gd_2WO_6 particles, indicating that an appropriate amount of Gd_2WO_6 could significantly reduce the recombination rate of photogenerated electrons and holes in ZnO. Consequently, this leads to a higher photocatalytic activity.

Photocatalytic degradation of Rh-B under different conditions with increasing irradiation times is displayed in Fig. 7. The dye was resistant to self-photolysis and for the same experiment with

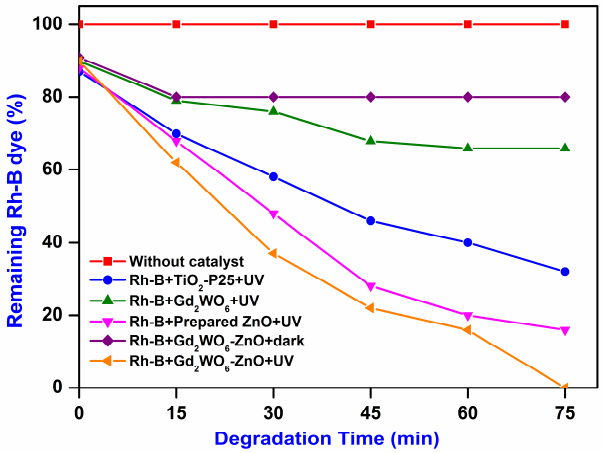

Fig 7–Photocatalytic degradation of Rh-B at varying irradiation times. [Rh-B conc. = 3×10^{-4} *M*; catalyst suspended = 3 g L^{-1}; pH = 7; airflow rate = 8.1 mL s^{-1}; irradiation time = 75 min, $I_{UV} = 1.381\times10^{-6}$ einstein L^{-1} s^{-1}].

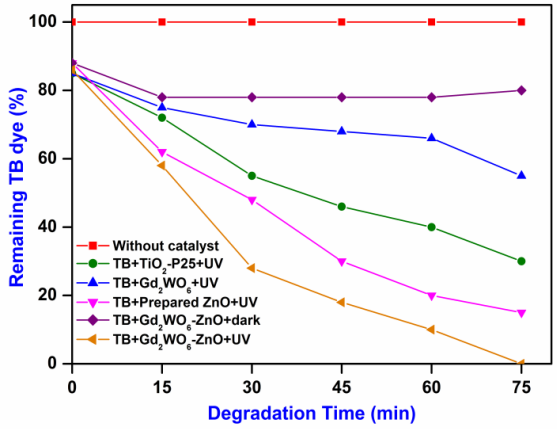

Fig 8–Degradation of tryptan blue by Gd_2WO_6-ZnO at varying irradiation times. [TB conc. = 1×10^{-4} *M*; catalyst suspended = 3 g L^{-1}; pH = 7; airflow rate = 8.1 mL s^{-1}; irradiation time = 75 min; $I_{UV} = 1.381\times10^{-6}$ einstein L^{-1} s^{-1}].

Gd_2WO_6-ZnO in the dark, a decrease (10%) in dye concentration was observed. This is because of the adsorption of dye on the catalyst. Rh-B undergoes complete degradation in the presence of Gd_2WO_6-ZnO under UV-A light in 75 min. However, the prepared ZnO, TiO_2-P25, and Gd_2WO_6 produced 84%, 69% and 36% degradations, respectively in 75 min. This shows that Gd_2WO_6-ZnO is most efficient in Rh-B degradation as compared to other photocatalysts (Fig. 7). Based on these results, it is obvious that the higher photocatalytic activity of Gd_2WO_6-ZnO is due to the loaded Gd_2WO_6. To test the effectiveness of the catalyst on the degradations of other dyes, we had carried out the experiments on the degradation of trypan blue (TB) under the same conditions. Figure 8 shows the percentages of

degradation of TB using Gd_2WO_6-ZnO at different irradiation times. TB undergoes 99% degradation in 75 min with Gd_2WO_6-ZnO. The results reveal that this catalyst is also efficient in the degradation of all azo dyes. UV spectral changes of Rh-B and TB at different irradiation times with Gd_2WO_6-ZnO catalyst are shown in Figs S3 and S4 (Supplementary data) respectively. There is a gradual decrease in intensity without the appearance of new absorption peaks.

The effect of pH on the photodegradation of Rh-B and TB was studied in the pH range 3–11 and the results are shown in Fig. S5. The degradation efficiency is high at pH 7 for both dye degradation and decreases when the pH is above or below 7. Low removal efficiency at acidic pH range may be due to the dissolution of ZnO in Gd_2WO_6-ZnO. Gd_2WO_6-ZnO is more advantageous than ZnO in the degradation of azo dyes Rh-B and TB because it has maximum efficiency at the neutral pH 7.

The reusability of Gd_2WO_6-ZnO was tested for the degradation of Rh-B and TB dyes under the same reaction environment. After complete degradation, the catalyst was separated and washed with deionised water. The recovered catalyst was dried in hot air oven at 100 ºC for 3 h and used for a second run. The outcome of degradation of Rh-B and TB for four successive runs is given in Fig. S6 (Supplementary data). Gd_2WO_6-ZnO gives 100, 98.0, 95.0 and 95.0% Rh-B degradation after 75 min in the first, second, third and fourth runs respectively, while for TB dye, 98, 96, 94 and 94% degradation respectively, was attained in 75 min. There is no change in the degradation efficiency of Gd_2WO_6-ZnO after third run.

As reported earlier[23,25,26] gadolinium doped materials display the highest photocatalytic activity. Gd^{3+} is half-filled with seven electrons in 4*f* shell. The half-filled electronic configuration is more stable. Under UV irradiation, it can be explained that the 4*f* level in gadolinium plays an important role in interfacial charge transfer and reduction of electron-hole recombination for gadolinium-doped sample.[23] Gd^{3+} ions act as an effective electron scavenger to trap the conduction band electrons of ZnO. In order to return back to its stable electronic configuration, gadolinium ions release the electrons to oxygen, which is reduced to form superoxide radicals. Furthermore, substitution of Zn^{2+} by gadolinium creates a charge imbalance, which is satisfied by the adsorption of more hydroxide ions on the surface of the catalyst.[27] The hydroxide ions act as hole traps

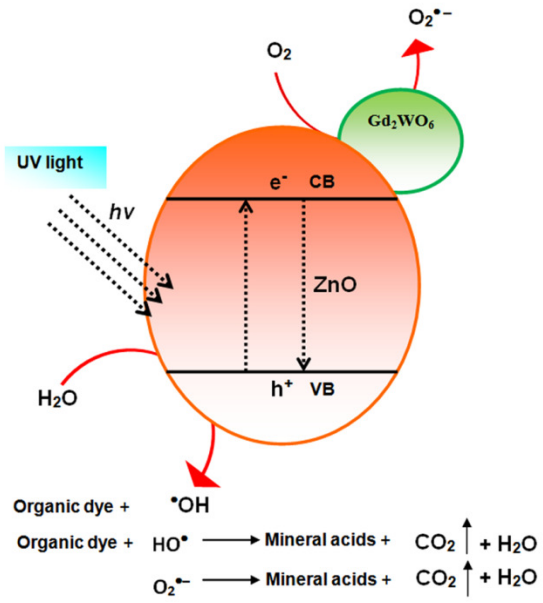

Scheme 1

that inhibit electron-hole pairs recombination and generate hydroxide radicals as well. Oxygen molecules adsorbed on the surface of the catalysts can easily react with the electrons released by gadolinium ions to form superoxide radicals, $O_2^{-\bullet}$. Superoxide radical ions ($O_2^{-\bullet}$) and the hydroxide radicals ($OH^{\bullet}$) generated by the reaction of the holes with hydroxide ions and water can promote the degradation of dye. (Scheme 1)

In summary, heterostructrued nanocrystalline Gd_2WO_6-ZnO photocatalyst was synthesized by a simple hydrothermal-thermal decomposition method and characterised by the various analytical techniques. The XRD pattern confirmed the distinct diffraction peaks of wurtzite ZnO and body-centered monoclinic structure of Gd_2WO_6 with good crystallinity. FE-SEM images showed that the catalyst exists as nanorod, nanocluster and microsponge-like structures with smooth surface. XPS analysis confirmed the homogeneous distribution of Gd, Zn, W and O in the prepared catalyst. Gd_2WO_6-ZnO was more efficient in the degradation of azo dyes, Rh-B and TB, as compared to the prepared ZnO, Gd_2WO_6, and TiO_2-P25. The enhanced photocatalytic activity was achieved by loading Gd_2WO_6 on ZnO. This catalyst. The presently synthesised Gd_2WO_6-ZnO nanocomposite was found to be stable and reusable and will be very useful as industrial green catalyst for the effective treatment of dye effluents.

Supplementary data

Supplementary data associated with this article, i. e., Figs S1– S6, are available in the electronic form at http://www.niscair.res.in/jinfo/ijca/IJCA_56A(01)50-56_SupplData.pdf.

Acknowledgement

Authors are thankful to the Council of Scientific & Industrial Research (CSIR), New Delhi, India, for financial support through research grant no. 02 (0144)/13/EMR–II.

References

1 Samadi M , Zirak M , Naseri A , Khorashadizade E & Moshfegh A Z, *Thin Solid Films,* 605 (2016) 2.
2 Rezaee A, Masoumbaigi H, Darvishi R, Khataee A R & Hashemiyand S, *Desalin Water Treat,* 44(1) (2012) 174.
3 Rashad M M, Ismail A A, Osama I, Ibrahim I A & Kandil A H T, *Arabian J Chem,* 7 (2014) 71.
4 Muruganandham M, Suri R P S, Sillanpaa M, Wu J J, Ahmmad B, Balachandran S & Swaminathan M, *J Nanosci Nanotechnol*, 14 (2014) 1898.
5 Jianxin W & Laitao L, *Catal Lett,* 126 (2008) 325.
6 Balachandran S, Prakash N, Thirumalai K, Muruganandham M, Sillanpaa M & Swaminathan M, *Ind Eng Chem Res,* 53 (2014) 8346.
7 Shi L, Lianga L, Ma J, Meng Y, Zhong S, Wang F & Sun J, *Ceram Int,* 40 (2014) 3495.
8 Faisal M , Ibrahim A A, Harraz F A, Bouzid H, Al-Assiri M S & Ismail A A, *J Mol Catal A: Chem,* 397 (2015) 19.
9 Wu W, Zhang S, Xiao X, Zhou J, Ren F, Sun L & Jiang C, *ACS Appl Mater Interfaces*, 4 (2012) 3602.
10 Balachandran S, Thirumalai K & Swaminathan M, *RSC Adv,* 4 (2014) 27642.
11 Glorieux B, Jubera V, Apheceixborde A & Garcia A, *Solid State Sci*, 13 (2011) 460.
12 Jambunathan V, Mateos X, Pujol M C, Carvajal J J, Diaz F & Aguilo M, *J Lumin,* 131 (2011) 2212.
13 Bantounas I, Singaravelu V, Roqan I S & Schwingenschlogl U, *J Mater Chem C*, 2 (2014) 10331.
14 Noel J L, Udayabhaskar R, Renganathan B, Muthu Mariappan S, Sastikumar D & Karthikeyan B, *Spectrochim Acta A*, 132 (2014) 634.
15 Ma X, *Thin Solid Films,* 520 (2012) 5752.
16 Baiju K V, Periyat P, Shajesh P, Wunderlich W, Manjumol K A, Smitha V S, Jaimy K B & Warrier K G K, *J Alloys Comp*, 505 (2010) 194.
17 Lei F, Yan B & Chen H H, *J Solid State Chem*, 181 (2008) 2845.
18 Kaczmarek A M & Deun R V, *Chem Soc Rev,* 42 (2013) 8835.
19 Zeng Y, Li Z, Wangab L & Xiong Y, *CrystEngComm*, 14 (2012) 7043.
20 Ansari S A, Khan M M, Ansari M O, Lee J & Cho M H, *J Phys Chem C,* 117 (2013) 27023.
21 Liu Y, Ai K, Yuan Q & Lu L, *Biomaterials*, 32 (2011) 1185.
22 Biloen P & Pott G T, *J Catal*, 30 (1973) 169.
23 Khataee A, Soltani R D C, Karimi A & Joo S W, *Ultrasonics Sonochem*, 23 (2015) 219.
24 Qing Z, Qingyu M, Yue T, Xiaohui F, Jiangting S & Shuchen L, *J Rare Earths*, 29(9) (2011) 815.
25 Tian N, Zhang Y, Huang H, He Y & Guo Y, *J Phys Chem C,* 118 (2014) 15640.
26 El-Bahy Z M, Ismail A A & Mohamed R M, *J Hazardous Mater,* 166 (2009) 138.
27 Wu Xu A W, Gao Y& Qin Liu H, *J Catal*, 207 (2002) 151.